Accelerated Disturbance Damping of an Unknown Distributed System by Nonlinear Feedback

Chien-Chong Chen and Hsueh-Chia Chang
Dept. of Chemical Engineering, University of Notre Dame, Notre Dame, IN 46556

We propose a new control design methodology for distributed systems with unknown nonlinear dynamics. The approach is appropriate for systems whose linearized differential operator possesses an eigenspectrum that can be partitioned into a low-dimensional slow spectrum and an infinite-dimensional fast complement. This separation of time scales allows us to utilize center manifold and normal form techniques of modern geometric theories for dynamical systems. It is shown that the convergence to an asymptotically stable equilibrium point after a small-amplitude transient disturbance quickly (exponentially fast) approaches an invariant manifold W *which is locally tangent to the eigenspace of the slow modes and is hence of the same dimension. The nonlinear dynamics on this invariant manifold is much slower than the fast approach and is dominated by the slow modes with the fast modes coupled "adiabatically" to them. The convergence can hence be best accelerated using a slow control with smooth nonlinear feedback involving only the slow modes. Nonlinear feedback is shown to drastically improve the performance of linear feedback. The only required information about the system in our approach is the slow adjoint eigenfunctions which can be easily estimated with a Karhunen-Loeve scheme for distributed systems. This identification scheme is quite robust to changes in process dynamics and can hence be carried out on-line in parallel with feedback control. The overall approach is verified by numerical experiments.*

Introduction

In addition to being extremely nonlinear and usually distributed, chemical systems often possess another important characteristic-their dynamic models are often inaccurate and incomplete. These three factors contribute to render stabilization or disturbance regulation problems of chemical systems exceedingly difficult. The conventional linear control theories, which presuppose a low-order linear model, identified through step, impulse or frequency response methods, are often inadequate. Realization of the importance of model uncertainties on closed-loop stability and performance has led to the recent advances in robust control theories (Morari and Zafiriou, 1989). Although the bulk of the work has been on linear systems, there has also been some attempts to extend the technique to nonlinear systems with proper definitions of norms on nonlinear operators. Nevertheless, robust control theories still begin with the premise that the plant model is almost perfect, that is, the modeling error is small. This is most certainly impossible to achieve for chemical systems whose modeling error measured by any norm is typically not small. This is especially true for an infinite-dimensional nonlinear distributed system.

It then seems pertinent to develop a control strategy for chemical systems that requires the least amount of information on the system dynamics. Preferably, this information can be easily identified on-line to account for the constantly varying conditions of most industrial operations. We introduce here an approach in this general direction. Gay and Ray (1986, 1988) have observed that the dynamics of a distributed system is often dominated by only a few dominant modes even though the system is infinite dimensional. This same concept also appears in hydrodynamics where "coherent structures" is the term coined for the dominant modes (Sirovich et al., 1990). These modes are simply the dominant eigenmodes of the linearized system differential operator if the nonlinear dynamics

Correspondence concerning this article should be addressed to H.-C. Chang.

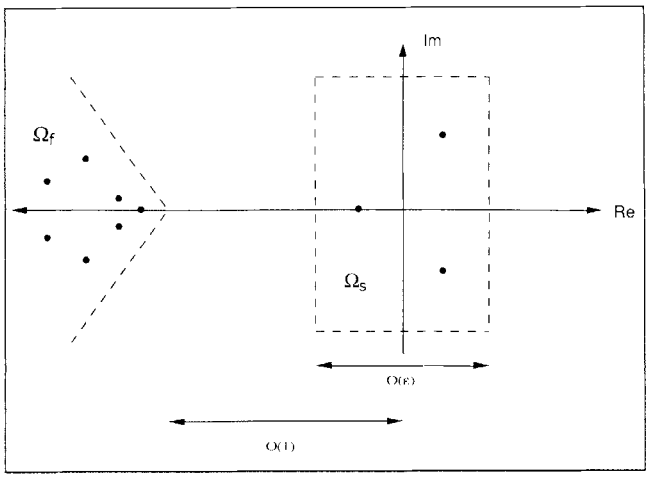

Figure 1. The spectrum of L with a slow subset Ω_s and a fast complement Ω_f.

is localized in a phase-space neighborhood of the equilibrium point such that the dominant modes are still represented by the leading eigenmodes in the presence of weak nonlinear effects. We shall restrict ourselves to such small-amplitude disturbances here and develop a weakly nonlinear control theory. In a sense, we replace the assumption of small modeling error in robust control theory with the assumption of small-amplitude disturbances. Recall that linear theories are only strictly valid for infinitesimal disturbances of truly nonlinear systems. Here, we permit weak nonlinear effects and our theory is hence an extension of linear control theories. A possible extension to a strongly nonlinear theory for more realistic disturbances will be discussed in the final section.

The existence of only a few dominant eigenmodes is a common property of chemical systems which contain a range of time scales. (See Aluko and Chang, 1984, for estimates of transport and kinetic time scales in a typical reactor.) For such systems, the infinite dimensions discrete spectrum of the linearized operator can be partitioned into two halves-a finite-dimensional slow (or dominant) spectrum Ω_s consisting of m slow (dominant, master) eigenvalues $\{\lambda_1, \lambda_2, ..\lambda_m\}$ and an infinite-dimension fast spectrum Ω_f containing the remaining fast (slave) eigenvalues $\{\lambda_{m+1}, \lambda_{m+2}, ...\}$. If more than two time scales exist, we shall only isolate the slowest one in Ω_s and lump all others in Ω_f. This partitioning is shown schematically in Figure 1. The eigenvalues λ_n are ordered by the index n in decreasing algebraic order of their real parts λ_n^r. In an earlier detailed modeling attempt of the autothermal reactor (McDermott and Chang, 1984; McDermott et al., 1985), we have obtained just such a partitioned spectrum. If we use $1/\lambda_{m+1}^r$ as a convenient characteristic time to scale our equations, then the distance of the fast eigenvalues from the imaginary axis is of O(1) or larger. The corresponding distance for Ω_s is then much smaller and is estimated by the parameter:

$$\epsilon = |\lambda_1^r/\lambda_{m+1}^r| \tag{1}$$

Our approach becomes increasingly accurate as $\epsilon \to 0$. We note that the eigenvalues in Ω_s can be either on the right or left half plane but they must be a distance of $O(\epsilon)$ from the imaginary axis. We shall also develop an empirical scheme to identify systems with a partitioned spectrum and to estimate ϵ.

A nonlinear system whose linearized operator yields a spectrum of the type shown in Figure 1 exhibits very unique nonlinear dynamics near the equilibrium point. Any sufficiently rich initial disturbance will excite all the modes in the spectrum. However, for small but finite-amplitude disturbances, the fast modes will relax very rapidly and the system trajectory will approach exponentially fast to an invariant manifold W of the same dimension as the number of slow eigenvalues. Hence, the convergence to the equilibrium point is dominated by the slow dynamics on W after a fast transient. Instead of modeling the entire infinite-dimensional nonlinear dynamics, one then needs only to decipher the low-dimensional and slow nonlinear dynamics on W. That a low-dimensional invariant manifold allows drastic dimension reduction has been exploited by Khorasani and Kokotovic (1986) and Kokotovic and Sauer (1989) for control purposes. The same concept has also been proposed in hydrodynamics where turbulence has been suggested to occur on a low-dimensional inertial or integral manifold (Foias et al., 1988; Titi, 1990; Teman, 1990).

In these previous studies, there was no stipulation that the dynamics occurs near an equilibrium point and the theories were in fact global. However, the very existence of such global invariant manifolds and whether they are attracting are difficult to ascertain even if the system is known exactly. Whether an attracting global invariant manifold exists for the Navier-Stokes equation, for example, remains a hotly pursued open problem (Titi, 1990). By restricting ourselves to local nonlinear dynamics here we ensure the existence and stability of W. Moreover, our approach will require only information of the local linear dynamics on W. Even the slow nonlinear dynamics is unnecessary. Hence, instead of reconstructing the actual nonlinear physical model, we shall only need the eigenfunctions and adjoint eigenfunctions of Ω_s. We shall show that these eigenfunctions will actually allow us to alter the nonlinear dynamics on W by using smooth nonlinear feedback with a slow control. Specifically, we shall accelerate the convergence of the system trajectory towards an asymptotically stable equilibrium point on W. If the equilibrium point is open-loop unstable, the feedback will also ensure its closed-loop asymptotic stability. We shall not estimate or alter the fast dynamics corresponding to the Ω_f spectrum. The reasons for not perturbing fast dynamics have been articulated by earlier work on the control of singularly perturbed systems.

Fast dynamics is difficult to estimate and model on-line. It is difficult to find fast actuators to respond to them. In our systems, the Ω_f spectrum dwells deep in the left half plane and hence relaxes very rapidly after excitation. There is hence no reason to alter the location of its fast eigenvalues. If fact, as we shall demonstrate, improper feedback may destabilize some eigenvalues in Ω_f and even move them into Ω_s or across the imaginary axis. This is highly undesirable and our feedback law will be designed to leave the Ω_f spectrum intact. It will only stabilize or shift the locations of the eigenvalues in Ω_s. Due to estimation error, high-gain feedback which shifts eigenvalues in Ω_s to Ω_f is also not advisable, as we shall also demonstrate. We hence stipulate that the closed-loop locations of the eigenvalues in Ω_s remain separated from Ω_f. Instead, we shall accelerate the slow dynamics on W by nonlinear feedback in addition to a weak linear one.

Isolating Ω_s from Ω_f in our feedback law requires accurate construction of the adjoint eigenfunctions $\{\hat{\phi}_i\}$ corresponding to Ω_s from an identification scheme. By virtue of their dominance, they are actually relatively easy to identify. However, one is still faced with the obstacle of resolving the spectrum, albeit only its dominant subset, of an unknown differential operator. The only feasible approach is to project the operator to a finite-dimension matrix operator and attempt to identify this matrix operator. This projection requires a set of optimal basis functions $\{\psi_i\}$ to decompose the signal during the identification stage. The closer the leading basis functions resemble the true dominant adjoint eigenfunctions $\{\hat{\phi}_i\}$, the fewer $\{\psi_i\}$ are required to reproduce the signal, the smaller the dimension of the matrix operator and the identification problem becomes easier. Consequently, one typically should not use spatial Fourier or orthogonal collocation decomposition insomuch as the true eigenfunctions rarely resemble them. See, for example, our computed eigenfunctions for the autothermal reactor (McDermott and Chang, 1984; McDermott et al., 1985). Instead, a statistically based procedure of experimentally extracting the most appropriate basis from the system directly will be used here. This basis set will be called the empirical eigenfunctions here and it is constructed by the proper orthogonal decomposition of Lumley (1970) which is also based on the method of Karhunen and Loeve (Loeve, 1955). We shall use the snap-shot version of Sirovich (1987). It will demonstrate through numerical experiments that only a handful (<5) of these empirical eigenfunctions are required to yield an excellent estimate of the true eigenfunctions and adjoint eigenfunctions. This then provides the final tool necessary for us to control nonlinear distributed systems with unknown dynamics.

Formulation

We consider the following nonlinear distributed system:

$$\dot{z} = L_x z + N(z) + \beta(x) u(t) \tag{2}$$

where z is an n-dimension vector function of the spatial variables x and the time variable t, $z = (z_1, z_2, ..z_n)$. We can treat the general case of three spatial dimensions $x = (x_1, x_2, x_3)$ but will use only one-dimensional examples. The overdot denotes time derivative as usual. The nonlinear term $N(z)$ contains z, its derivatives with respect to x and perhaps even x explicitly. We shall assume that the original equation has been properly reduced with respect to a possible nonhomogeneous equilibrium state, which has been chosen to be set point, such that

$$N(0) = 0 \tag{3}$$

that is, the origin $z = 0$ is always an equilibrium state of the reduced problem in Eq. 2. Our results actually apply to the general case of $N(z, u)$ as we shall demonstrate subsequently. It is, however, more convenient to present the approach with the simpler case of $N(z)$. The input variable $u(t) = (u_1, u_2, \ldots u_k)$ is a k-dimensional spatially uniform vector. To ensure that every eigenvalue in Ω_s can be independently shifted by feedback, we shall assign k to be the "codimension" of the Ω_s spectrum, that is, the number of real eigenvalues plus the number of complex conjugate pairs. Hence, if $m = 2$ and the two slow eigenvalues are real, then $k = 2$. However, if $m = 2$ and the two slow eigenvalues are a complex pair, then $k = 1$. We shall only examine the codimension $k = 1$ case here for $m = 1$ and 2. The $n \times k$ matrix function $\beta(x)$ is a function of the spatial variable x only. For $k = 1$, it is a vector function, $\beta(x) = (\beta_1, \beta_2, \ldots \beta_n)$ and u is a scalar input variable.

The linear differential operator L_x is an $n \times n$ differential operator and it defines the following eigenvalue and adjoint eigenvalue problems:

$$L_x \phi_i = \lambda_i \phi_i \tag{4a}$$

$$L_x^+ \hat{\phi}_i = \bar{\lambda}_i \hat{\phi}_i \tag{4b}$$

where the bar denotes complex conjugate and L_x^+ defines the adjoint operator with respect to the usual L_2 inner-product, $(f, g) = \int f \cdot g \, dx$:

$$(L_x y, z) = (y, L_x^+ z) \tag{5}$$

Both Eqs. 2, 4, and 5 must be complemented by an appropriate set of homogeneous boundary conditions. They are homogeneous because, like Eq. 3, we assume that a reduction with respect to an equilibrium state has been carried out. We assume, for simplicity, that these boundary conditions are linear in the reduced variable z and are independent of u. Both are true in most systems although our approach can be readily extended to the exceptional cases. Specific mention of these boundary conditions will be omitted in subsequent discussion.

The spectrum of L_x, $\Omega(L_x)$, has been assumed to be discrete and infinite-dimensional. Although the center manifold theories we utilize can be extended to operators with a continuous spectrum (Crawford, 1984), we shall avoid this more esoteric case here. As mentioned, Ω is partitioned into the two halves in Figure 1:

$$\Omega = \Omega_s \cup \Omega_f \tag{6}$$

with the first m eigenvalues in Ω_s. We shall expand z by $\{\phi_i\}$:

$$z(x, t) = \sum_{i=1}^{\infty} a_i(t) \, \phi_i(x) \tag{7}$$

Substituting Eq. 7 into Eq. 2 and taking inner product with $\hat{\phi}_j$, we obtain from the projection, due to the biorthogonality between the eigenfunctions and the adjoint eigenfunctions, the following dynamical systems for the amplitudes $a_i(t)$ describing the projection of the dynamics on the ϕ_i basis:

$$\dot{a}_s = \Lambda_s a_s + f(a_s, a_f) + b_s u \tag{8a}$$

$$\dot{a}_f = \Lambda_f a_f + g(a_s, a_f) + b_f u \tag{8b}$$

where $a_s = (a_1, a_2, \ldots a_m)$ are the amplitudes of the slow modes and $a_f = (a_{m+1}, \ldots)$ denotes the amplitudes to the rest of the spectrum, Ω_f. Note that since ϕ_i and λ_i can be complex, the amplitudes can also be complex. The matrices Λ_s and Λ_f are simply diagonal matrices with the slow and fast eigenvalues on their diagonals. Due to the separation of the spectrum shown in Figure 1, the real parts of the diagonal terms λ_i in

Λ_s are of $O(\epsilon)$. The constant matrices b_s and b_f are simply projection of $\beta(x)$ onto the eigen sub spaces Ω_s and Ω_f:

$$[b_s]_{pq} = (\beta \cdot \hat{e}_q, \hat{\phi}_p) \quad p = 1,2,\ldots, m; \quad q = 1,2,\ldots,k \tag{9a}$$

$$[b_f]_{pq} = (\beta \cdot \hat{e}_q, \hat{\phi}_p) \quad p = m+1,\ldots; \quad q = 1,2,\ldots,k \tag{9b}$$

where $\hat{e}_q$ is the k-dimensional unit vector whose qth element is unity and all other elements are zero. We shall assume all the slow eigenvalues in Ω_s are controllable (affected by feedback) and hence (Λ_s, b_s) is a controllable pair. The projected nonlinearity must be treated with more care since $N(z)$ in Eq. 2 can contain spatial derivatives of z. We shall follow the notation of Iooss and Joseph (1980) and define:

$$D[y_1, y_2] = \frac{1}{2} \frac{\partial^2}{\partial\delta_1 \partial\delta_2} N(\delta_1 y_1 + \delta_2 y_2)|_{\delta_1 = \delta_2 = 0} \tag{10a}$$

$$T[y_1, y_2, y_3] = \frac{1}{3!} \frac{\partial^3}{\partial\delta_1 \partial\delta_2 \partial\delta_3} N(\delta_1 y_1 + \delta_2 y_2 + \delta_3 y_3)|_{\delta_1 = \delta_2 = \delta_3 = 0} \tag{10b}$$

Higher-order expansions can likewise be defined. The nonlinear terms $f(a_s, a_f)$ and $g(a_s, a_f)$ in Eq. 8, where $f(0, 0) = 0$ and $g(0, 0) = 0$, are then to leading order:

$$f(a_s, a_f) \sim B \cdot a_s \cdot a_s + C \cdot a_s \cdot a_f + D \cdot a_f \cdot a_f + E \cdot a_s \cdot a_s \cdot a_s \tag{11a}$$

$$g(a_s, a_f) \sim F \cdot a_s \cdot a_s \tag{11b}$$

where

$$B_{ijk} = \frac{\partial^2}{\partial(a_s)_j \partial(a_s)_k} (D[a_s, a_s], \hat{\phi}_i) \; i, j, k = 1,\ldots, m \tag{12a}$$

$$C_{ijk} = 2 \frac{\partial^2}{\partial(a_s)_j \partial(a_f)_k} (D[a_s, a_f], \hat{\phi}_i) \; i, j = 1, \ldots, m; \; k = m+1,\ldots \tag{12b}$$

$$D_{ijk} = \frac{\partial^2}{\partial(a_f)_j \partial(a_f)_k} (D[a_f, a_f], \hat{\phi}_i) \; i = 1, \ldots, m; \; j, k = m+1,\ldots \tag{12c}$$

$$E_{ijkl} = \frac{\partial^3}{\partial(a_s)_j \partial(a_s)_k \partial(a_s)_l} (T[a_s, a_s, a_s], \hat{\phi}_i) \; i, j, k, l = 1, \ldots, m \tag{12d}$$

$$F_{ijk} = \frac{\partial^2}{\partial(a_s)_j \partial(a_s)_k} (D[a_s, a_s], \hat{\phi}_i) \; i = m+1, \ldots; \; j, k = 1,\ldots, m \tag{12e}$$

The omitted terms in Eq. 11 are higher-order amplitude terms unnecessary in the resolution of our closed-loop equation using weakly nonlinear feedback.

We shall now analyze the projected system Eq. 8 by center manifold theory. The open-loop case $u = 0$, will be studied first. Since the real parts of the elements of Λ_s are of $O(\epsilon)$, we shall decompose it as:

$$\Lambda_s = \epsilon \Lambda_r + i \Lambda_i \tag{13}$$

where Λ_r and Λ_i are real matrices with elements of $O(1)$. We shall first look at the limit of $\epsilon = 0$ and examine

$$\dot{a}_s = i \Lambda_i a_s + f(a_s, a_f) \tag{14a}$$

$$\dot{a}_f = \Lambda_f a_f + g(a_s, a_f) \tag{14b}$$

Then according to the center manifold theory (Carr, 1981; Guckenheimer and Holmes, 1983), there exists an m-dimensional invariant manifold called the center manifold M which contains the origin and is tangent to all the slow eigenvectors $a_s = 0$ at the origin. This center manifold M is given by:

$$a_f = h(a_s) \tag{15}$$

and the dynamics on M is described by the slow equation:

$$\dot{w} = i\Lambda_i w + f(w, h(w)) \tag{16}$$

which is obtained by substituting Eq. 15 into Eq. 14a. The expression in Eq. 15 is sometimes called adiabatic coupling or slave-master coupling and it depicts how the fast modes are coupled nonlinearly to the slow modes in the slow dynamics on M. The center manifold M is an invariant manifold because any initial condition on M yields a trajectory that remains on M for all time. Using this fact that $a_f = h(a_s)$ must be invariant under the flow of Eq. 16, we can construct h by:

$$\dot{a}_f = \frac{d}{dt} h(a_s) = \nabla_s h(a_s) \cdot [i \Lambda_i a_s + f(a_s, h(a_s))]$$
$$= \Lambda_f h(a_s) + g(a_s, h(a_s)) \tag{17}$$

where ∇_s represents the gradient operator with respect to a_s. The two sides of the last equality in Eq. 17 allows us to construct $h(a_s)$ in a Taylor expansion of a_s provided coefficients of the same order are also available in f and g from Eq. 11. Not only does the center manifold theorem stipulates the existence of M and permits its construction, it also ensures that M is attracting. More specifically, given an initial condition (a_s (0), a_f (0)) sufficiently small, the solution of Eq. 8 with this initial condition converges to M with an exponential rate related to λ^r_{m+1}, the real part of the leading eigenvalue in Ω_f:

$$a_s(t) = w(t) + O(e^{\lambda^r_{m+1} t}) \tag{18a}$$

$$a_f(t) = h(w(t)) + O(e^{\lambda^r_{m+1} t}) \tag{18b}$$

where w is given by the manifold dynamics of Eq. 16.

We shall examine the simplest cases of unit codimension ($k = 1$) with a dominant real mode ($m = 1$) or a dominant complex pair ($m = 2$) here. In the first case, the scalar amplitude a_s is real and one obtains from Eq. 16 the governing slow equation for the dynamics on M to $O(w^3)$:

$$\dot{r}_1 = \gamma_2 r_1^2 + \gamma_3 r_1^3 + O(r_1^4) \tag{19}$$

where the real coefficients are simply:

$$\gamma_2 = B \tag{20a}$$

$$\gamma_3 = E - C \cdot (\Lambda_f^{-1} F) \tag{20b}$$

and we have replaced a_s by r_1 for convenience. We note that from Eq. 7 the amplitude of the dominant mode is simply:

$$r_1(t) = a_1(t) = (z, \hat{\phi}_1) \tag{21}$$

For the complex case, the two dominant eigenmodes are complex conjugates and $\lambda_{1,2}^i = \pm i\omega$.
The projected Eq. 16 has the form:

$$\dot{w} = i\omega w + \alpha_1 w^2 + \alpha_2 w\overline{w} + \alpha_3 \overline{w}^2 + \alpha_4 w^3 + \alpha_5 w^2 \overline{w} + \alpha_6 w \overline{w}^2 + \alpha_7 \overline{w}^3 \tag{22}$$

where

$$\alpha_1 = B_{111} \qquad \alpha_2 = B_{112} + B_{121}$$
$$\alpha_3 = B_{122} \qquad \alpha_4 = E'_{1111}$$
$$\alpha_5 = E'_{1112} + E'_{1121} + E'_{1211} \qquad \alpha_6 = E'_{1122} + E'_{1212} + E'_{1221}$$
$$\alpha_7 = E'_{1222} \tag{23}$$

where

$$E'_{klmn} = E_{klmn} + \sum_{p \in \Omega_f} C_{klp} F_{pmn} / \{2i\omega - (\lambda_f)p\}$$

and $(\lambda_f)_p$ is the pth fast eigenvalue. The amplitude w is complex here and Eq. 21 and its conjugate then describe the dynamics on M. For this complex case, Eq. 22 can be further simplified with a near-identity nonlinear transformation of w using normal form theory (Guckenheimer and Holmes, 1983). This smooth coordinate transform:

$$w = v + \phi(v) \tag{24}$$

where $\phi(v) \sim O(|v|^2)$ does not alter the qualitative behavior of the dynamics on M. Also, since it is a near-identify transformation $\phi(v) \ll v$, the leading order quantitative estimate remains valid. We eschew the detailed Lie algebra involved for transforming Eq. 22 and refer the readers to our earlier derivation (Hwang and Chang, 1987) of the following formulae. Using a cylindrical coordinate

$$v = r_2 e^{i\theta} \tag{25}$$

one can use Eq. 22 to transform the slow equation Eq. 22 to a real amplitude equation and a phase equation:

$$\dot{r}_2 = \gamma_3 r_2^3 + O(r_2^5) \tag{26a}$$

$$\dot{\theta} = \omega + O(r_2^2) \tag{26b}$$

where γ_3, like Eq. 20a, is also a real coefficient given by

$$\gamma_3 = 1/8\ [3g_1 + g_2 + g_3 + 3g_4] + 1/(8\omega)\ [g_5(g_6 + g_7) - g_8(g_9 + g_{10}) - 2\ g_6 g_9 - 2\ g_7 g_{10}] \tag{27}$$

where

$$g_1 = \alpha'_4 + \alpha'_5 + \alpha'_6 + \alpha'_7 \qquad g_2 = -3\alpha'_4 + \alpha'_5 + \alpha'_6 - \alpha'_7$$
$$g_3 = 3\alpha'_4 + \alpha'_5 - \alpha'_4 - 3\alpha'_4 \qquad g_4 = -\alpha'_4 + \alpha'_5 - \alpha'_6 + \alpha'_7$$
$$g_5 = -2\alpha'_1 + 2\alpha'_3 \qquad g_6 = \alpha'_1 + \alpha'_2 + \alpha'_3$$
$$g_7 = -\alpha'_1 + \alpha'_2 - \alpha'_3 \qquad g_8 = 2\alpha'_1 - 2\alpha'_3$$
$$g_9 = \alpha'_1 + \alpha'_2 + \alpha'_3 \qquad g_{10} = -\alpha'_1 + \alpha'_2 + \alpha'_3$$

Here, the amplitude $r_2(t)$ can again be extracted from an instantaneous measurement of $z(x, t)$ by:

$$r_2(t) = |(z, \hat{\phi}_1)| \tag{28}$$

where $|\cdot|$ is the complex norm, $|w|^2 = (Re\{w\})^2 + (Im\{w\})^2$ for any complex number w. Equations 19 and 26a hence describe the nonlinear dynamics on M for the idealized limit of $\epsilon = 0$. We note that the amplitude Eq. 26a for a complex dominant pair contains no quadratic term as in Eq. 19. This is related to the well-known fact that a Hopf bifurcation is always a pitchfork bifurcation while a simple one is a transcritical one in general. In summary, when $\epsilon = 0$, the perturbed system will relax rapidly (exponentially in time with rate λ'_{m+1}) and converge to the center manifold M whose nonlinear dynamics is described by Eqs. 19 or 26 for $m = 1$ or 2, respectively. Since there is no linear dynamics for this idealized limit, the dynamics on M remains nonlinear for all time, that is, one will never see an exponential decay to the equilibrium point on M. Nevertheless, the origin can still be asymptotically stable such that the dynamics on M eventually converges to the origin as $t \to \infty$ if γ_2 is sufficiently small or γ_3 is sufficiently negative in Eqs. 19 and 26a. These results can be easily verified by using the Lyapunov function $V = 1/2\ r_i^2$ for $i = 1$ or 2. Of course, γ_3 can be positive or not sufficiently negative such that the origin is not asymptotically stable or the system may converge to the origin at an unsatisfactory slow rate. We shall then use nonlinear feedback in r_i of Eqs. 21 or 28 to accelerate the dynamics.

The discussion of the feedback law can be conveniently combined with the relaxation of the vanishing ϵ idealization. Recall first we only shift the dominant eigenvalues with Ω_s. This then stipulates that the linear feedback must be weak and one must have

$$u(t) = -\epsilon k_L r_i - k_N r_i^3 \quad i = 1 \text{ or } 2 \tag{29}$$

where r_i is the amplitude of the dominant modes given by Eqs. 21 or 28 and k_L and k_N are then $O(\epsilon^0) = O(1)$ linear and nonlinear gains respectively. The scaled linear gain k_L is of unit order since it is already premultiplied by ϵ. It is related to the true gain by

$$k'_L = \epsilon k_L \tag{30}$$

The nonlinear feedback does not contain a quadratic r^2 term because like γ_2 in Eq. 19, a quadratic feedback will only disrupt the asymptotic stability of the origin. One can attempt to cancel the quadratic term in Eq. 19 exactly by using quadratic feedback but this involves an accurate estimation of the γ_2 coef-

ficient. This value must be obtained from the nonlinear dynamics on M and is hence difficult to decipher. We shall retain the odd feedback law of Eq. 29 where k_L and k_N do not need to take on precise values. The nonlinear feedback $k_N r^3$ will be used to offset any undesirable effect of the quadratic term. We note that nonlinear feedback which attempts to cancel all the nonlinear terms in the system would essentially be equivalent to a local version of linearizing control (Kravaris and Kantor, 1990).

Since nonlinear feedback does not have to be weak, we shall use the maximum allowed by our formulation, $k_N \sim O(1)$. Inserting Eq. 29 into Eq. 8 and stipulating that we are in the neighborhood of the origin where $r \sim O(\epsilon^{1/2})$, one can use an "extended" trick of Guckenheimer and Holmes (1983) to obtain the extension of Eqs. 19 and 26 to closed-loop systems with finite ϵ. We omit the details here and simply present the final results for the closed-loop slow equations:

$$\dot{r}_1 = \epsilon(\lambda_1' - k_L b) r_1 + \gamma_2 r_1^2 + (\gamma_3 - k_N b) r_1^3 \tag{31a}$$

$$\dot{r}_2 = \epsilon(\lambda_1' - k_L b) r_2 + (\gamma_3 - k_N b) r_2^3 \tag{31b}$$

where

$$b = Re\ \{(\beta, \hat{\phi}_1)\} \tag{32}$$

which is a scalar for this codimension one case (β is a n-dimensional vector function and u is a scalar input).

Equations 31 describe the nonlinear dynamics on an invariant manifold W which is actually identical to leading order to the center manifold M of the open-loop case with $\epsilon = 0$. The reasoning invokes some order arguments. We first note that the weak linear feedback does not affect the eigenvalues in Ω_f to leading order. An examination of Eq. 8 with Eq. 29 shows that the closed-loop eigenvalues in Ω_s are $\epsilon(\lambda_1' - k_L b) + O(\epsilon^2)$ while the closed-loop Ω_f spectrum remains intact at the leading order $O(\epsilon^0)$. If, however, our estimate of $\hat{\phi}_1$ is imperfect such that the feedback law Eq. 29 contains some small $O(\delta)$ contribution from the fast modes, $u = -\epsilon k_L a_1 - k_N a_1^3 - \epsilon\delta k_L a_j$ where $a_j \in \Omega_f$, the closed-loop Jacobian is not diagonal and is instead filled by terms of $O(k_L \delta\epsilon)$ at the off-diagonal positions. These small terms due to estimation error do not change the above leading order conclusions about the closed-loop eigenvalues except at large gain such that $\epsilon\delta\ k_L \sim O(\epsilon)$ and closed-loop coupling occurs between the slow and fast modes. This robustness consideration stipulates that k_L must be of $O(1)$ or k'_L must be small to ensure decoupling. Weak linear feedback also explains why W and M are equivalent to leading order. The resolution of our slow Eqs. 19 and 26a is only to third order in the amplitude of the slow modes a_s. Since $a_f \sim O(|a_s|^2)$ to leading order in the center manifold projection of Eq. 15, the only term that the center manifold projection affects in the third-order slow equation of Eq. 14a is the term $a_s a_f$ in Eq. 14a. This implies that we only need to resolve h to $O(|a_s|^2) \sim O(r^2)$ from Eq. 17. Insomuch as feedback and ϵ terms contribute leading order terms of order ϵa_s and a_s^3 to Eq. 8b, which are both of $O(r^3)$, they do not change the $O(r^2)$ terms in Eq. 17 and M is identical to W to second order. Although linear terms of $O(\epsilon)$ and nonlinear feedback by Eq. 29a do not alter the invariant manifold to second order, that is, $h(a_s)$ remains the same as before, the dynamics on W as governed by Eqs. 19 and 26a are affected by them. They give rise to the first two terms and the last term of Eq. 31. We can hence alter the dynamics on M by dominant mode feedback.

Also using the same order arguments, it can be shown that Eq. 31 remains valid to leading order for the general case of $N(z, u)$. The extra terms of order $a_s u$, u^2, $a_f u$ and higher in Eq. 8 all lead to terms of order r^4 or higher in Eq. 31 since $u \sim O(\epsilon r) \sim O(r^3)$. The invariant manifold is also unaltered to $O(r^2)$. This is an important consequence of weak linear feedback. We also note from Eq. 31b that for the complex case, linear feedback only alters the real part of the dominant complex mode. This is because our feedback law Eq. 29 involves only the amplitude of the deviation variable. If phase is added to the feedback law, the imaginary part and hence the closed-loop dominant frequency will also be altered by the feedback. As a result, Eq. 26b becomes:

$$\dot{\theta} = \omega - k_L' Im\ \{(\beta, \hat{\phi}_1)\} \tag{33}$$

to leading order, where k_L' is the gain for the phase feedback. However, since the closed-loop phase equation remains decoupled from the amplitude equation, Eq. 31 is still valid under this more elaborate feedback.

A major advantage of our feedback law Eq. 29 is that the only required information is $\hat{\phi}_1$ to evaluate r_i from Eq. 21 or Eq. 28. Yet we can affect the nonlinear dynamics on W. It is also necessary to ensure that $k_L b$ is positive but this typically requires only simple tuning. We note from Eq. 31 that the nonlinear gain k_N must be of the same sign as the linear gain k_L if accelerated convergence and enhanced asymptotic stability are desired. Writing Eq. 31 collectively as

$$\dot{r} = -\mu r + \delta_2 r^2 - \delta_3 r^3 \tag{34}$$

where μ and δ_3 are positive, we can immediately decipher the asymptotic stability of the origin. The Lyapunov function $V(r) = 1/2\ r^2$ yields that asymptotic stability is ensured ($\dot{V} < 0$) if

$$-\mu + \frac{\delta_2^2}{4\ \delta_3} < 0 \tag{35}$$

Consequently, asymptotic stability is always ensured for Eq. 31b where $\delta_2 = 0$ and is guaranteed for Eq. 31a if:

$$\delta_3 > \frac{\delta_2^2}{4\ \mu} = \delta_3^c \sim O(\epsilon^{-1}) \tag{36}$$

It is hence to our advantage to use high-gain nonlinear feedback in both cases. However, because of the assumptions we have made regarding the order of k_N, it cannot be more than unit order with respect to ϵ. Higher k_N will lead to nonlinear coupling between the fast and slow modes. However, k_N of $O(1)$ already dramatically accelerates the convergence towards the origin. We demonstrate this without the quadratic term δ_2 in Eq. 34. The resulting equation is commonly known as the Stuart-Landau equation and δ_3 is called the Landau constant. It applies to the slow dynamics after the system has converged onto W (regions II and III in Figure 2). In region III near the origin, where r is of smaller order then $\epsilon^{1/2}$ ($r \sim O(\epsilon)$ say), the linear term dominates over the cubic term and the system

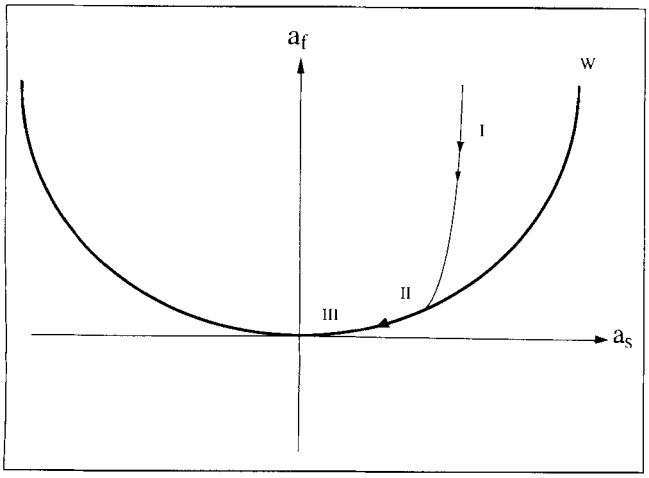

Figure 2. The convergence of a trajectory onto the invariant manifold *W* in a schematic fast and slow mode phase plane.

Region I corresponds to the fast exponential decay of the fast mode. Region II involves $O(r^3)$ nonlinear dynamics on W and region III pertains the final slow linear dynamics near the origin.

decays exponentially by the linear dynamics $r \sim \exp(-\mu t)$. However, at the beginning of region II, where the perturbation is such that r is larger order than $\epsilon^{1/2}$ (say $O(\epsilon^{1/4})$), then the cubic term dominates the linear term and r decays algebraically, $r \sim (\delta_3 t)^{-1/2}$. (In the region where $r \sim O(\epsilon^{1/2})$, both linear and nonlinear terms are of the same order. The algebraic region lies right at the edge of this neighborhood where our slow equations are valid.) It is in the algebraic region where linear feedback has no influence over the dynamics and only nonlinear feedback can accelerate the algebraic decay through the effect of k_N on δ_3. This is sketched schematically in Figure 3 where the importance of nonlinear feedback on relatively large-amplitude disturbances is emphasized. The convergence rate is greatly accelerated by nonlinear feedback because it is felt much further away from the origin than linear feedback.

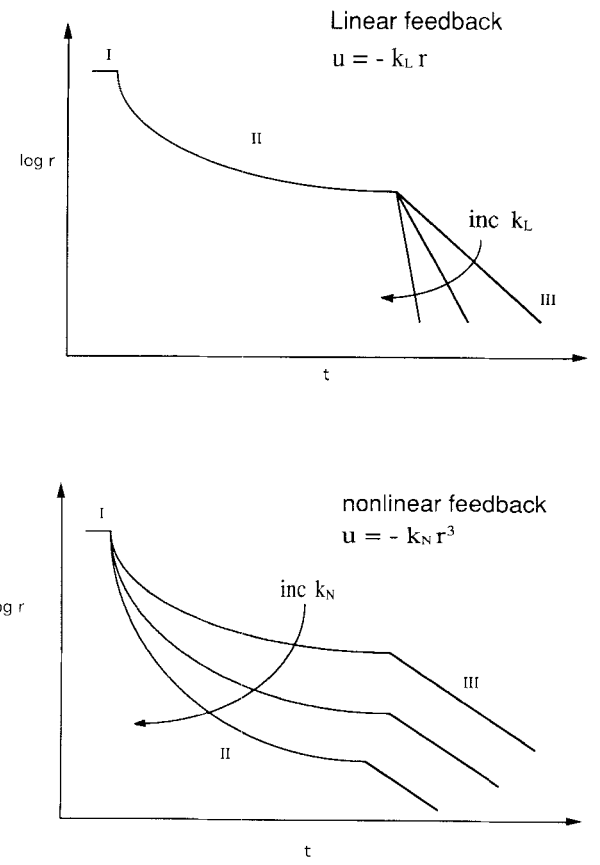

Figure 3. Schematic time evolution of the slow variable under feedback control.

Linear feedback increases the exponential decay rate of the final linear region III while nonlinear feedback modulates large-amplitude disturbances and provides a far better performance.

Identification of Dominant Adjoint Eigenfunctions

For the codimension 1 case ($k=1$), the input u is a scalar spatially uniform function and the only required information is $\hat{\phi}_1(x)$ which is real for $m=1$ and complex for $m=2$. We shall develop an indentification scheme for this dominant adjoint eigenfunction here. We begin by decomposing the experimental data z with a convenient orthonormal basis $\{\Psi_n\}$:

$$z_N(x, t) = \sum_{i=1}^{N} c_i(t)\, \psi_i(x) \tag{37}$$

For accuracy, the error $\|z - z_N\|_2$ must be small where $\|\cdot\|_2$ is the L_2 norm $(\cdot,\cdot)^{1/2}$. If z is approximated well by z_N, the dominant linear dynamics of Eq. 2 can be deciphered from the time series of the coefficients:

$$c_n(t) = (z, \psi_n) \tag{38}$$

by constructing the linear map A relating the vector of expansion coefficients $c(t) = (c_1(t), c_2(t), .. c_N(t))$ to $c(t+\Delta t)$ $= (c_1(t+\Delta t), c_2(t+\Delta t), .. c_N(t+\Delta t))$, where Δt is an assigned time step:

$$c(t+\Delta t) = Ac(t) \tag{39}$$

the $N \times N$ matrix A is simply a discrete time version of the projection $\tilde{A}$ of the operator L_x using $\{\psi_i\}$ as a basis:

$$\tilde{A}_{ij} = (L_x \psi_j, \psi_i) \tag{40}$$

$$\tilde{A} = (\ln A)/\Delta t \tag{41}$$

The matrix A is then estimated from the time series by minimizing the following cost function with respect to the elements of A:

$$J = \sum_l \| c((l+1)\Delta t) - A \cdot c(l\Delta t) \|^2 \tag{42}$$

where $\|\cdot\|$ is the Euclidean norm, to yield:

$$A = PQ^{-1} \tag{43}$$

where the $N \times N$ matrices P and Q are:

$$P=\sum_l c((l+1)\Delta t)c(l\Delta t) \tag{44a}$$

$$Q=\sum_l c(l\Delta t)c(l\Delta t) \tag{44b}$$

After obtaining A, the projected operator $\tilde{A}$ can then be obtained from Eq. 41. However, directly using Eq. 41 to obtain $\tilde{A}$ is not advisable, because it involves matrix logarithm which requires large computing time to converge. Since we only need the eigenvalues and eigenvectors of $\tilde{A}$, they can be obtained from A instead of $\tilde{A}$ based on the following relationship:

$$\tilde{\lambda}(\tilde{A})=[ln\lambda(A)]/\Delta t$$

$$\{\tilde{v}(\tilde{A})\}=\{v(A)\}$$

The eigenvalues $\tilde{\lambda}_n$ of $\tilde{A}$ are then simply the eigenvalues of L_x and its eigenvectors $\{v_n\}$ and adjoint eigenvectors $\{\hat{v}_n\}$ provide the dominant eigenfunctions and adjoint eigenfunctions of L_x:

$$\phi_n(x)=\sum_{i=1}^{N}[v_n]_i\psi_i(x) \tag{45a}$$

$$\hat{\phi}_n(x)=\sum_{i=1}^{N}[\hat{v}_n]_i\psi_i(x) \tag{45b}$$

This completes our estimates of the dominant adjoint eigenfunctions.

There are several important considerations in the above scheme. We have refrained from a detailed analysis of the optimal sampling period Δt. However, it is quite apparent that it should be longer than the noise time scale such that the distributed signal $z(x, t)$ reflects the true system dynamics and pattern and not that of the disturbance. On the other hand, it should not be longer than the dominant system time scale $1/\lambda_1^r$ lest the dominant dynamics is not captured. Not knowing the noise and system time constant a priori, the optimal sampling time must hence be obtained empirically. An inappropriate sampling time would require a longer time series for accurate identification. A more detailed analysis of the optimal sampling period for a given length of time series can perhaps be based on a minimization of J in Eq. 42. This seems difficult, however, without a priori information on the system (model). Another important point is that since the signal z in Eq. 39 must be a reduced variable, we need to estimate that unreduced equilibrium state empirically and carry out the reduction online. As we shall demonstrate, the equilibrium state is best obtained by time-averaging the measured unreduced variables under relatively quiescent conditions for open-loop stable systems with at most small-amplitude random noise. For oscillatory systems with an unstable equilibrium state, only an approximation can be obtained by averaging the nonlinear oscillations. After reduction, one is faced with the choice of selecting N in Eq. 37 for a given basis set. The estimate of A in Eq. 43 is more accurate with a small N. However, N must be large enough such that z_N is a good approximation of z. It seems then one should use as large an N as possible and utilize sufficient time series data to obtain an accurate estimate of A. If the spectrum of A (or L_x) is indeed partitioned, this would then be revealed by the spectrum of A and we can then decipher the number of dominant modes m and only use their corresponding adjoint eigenfunctions in our feedback. We shall demonstrate, however, that by using an optimal basis set $\{\psi_i\}$, the empirical eigenfunctions, the number of dominant modes m can be deciphered a priori. In fact, an empirical criterion for identifying systems with the partitioned spectrum of Figure 1 will be introduced. Using these empirical eigenfunctions, the number N used in the estimation scheme can be minimized, thus facilitating the identification of the true adjoint eigenfunctions. It should also be noted that $\hat{\phi}_1$ can only be obtained from the linear dynamics. Care must hence be taken such that the time series $c(l\Delta t)$ is close to the equilibrium state. Moreover, this set of data should be noise-free since noise tends to camouflage the dynamics. These are two conflicting requirements since small-amplitude signal tends to be sensitive to noise. We have found that the best data are obtained from large-amplitude step change responses. We isolate the linear dynamics of this response by noting when the trajectory of $c(t)$ has converged onto a plane containing the origin. This plane corresponds to the projected eigenspace in the coordinates of the $\{\psi_i\}$ basis. (It corresponds to region III of Figure 2). If the time series is corrupted by noise before convergence to this plane, more quiescent conditions or noise-filtering techniques would then be necessary. We shall demonstrate this scheme in the examples but simply note here that the step response data necessary for estimating A are different from the noise-sustained data for estimating the equilibrium state and the empirical eigenfunctions.

We first tackle the problem of estimating the equilibrium state to allow reduction. Let $z_l'(x)=z'(x,l\Delta t)$ be a distribution time series (snapshots) of the unreduced raw variable from the response of the system to random distributed noise. We assume an infinite array of sensors along x. If there is only a finite number, some spatial smoothing and intrapolation using perhaps orthogonal collocation are assumed to have been carried out. We assume here the measurement and smoothing errors are small. The equilibrium state can then be estimated from a time averaging of the time series.

$$\bar{z}'(x)=\lim_{M\to\infty}\frac{1}{M}\sum_{l=1}^{M}z_l'(x) \tag{46}$$

and a reduced time series $z_l(x)=z_l'(x)-\bar{z}'(x)$ can then be constructed. If the noise is truly random such that the ergodic hypothesis can be invoked, the time series $\{z_l(x)\}$ is a random ensemble of the system response and the time average operation in Eq. 46 is equivalent to an ensemble average $\langle\cdot\rangle$.

A two-point spatial correlation function $K(x,x')$ is then defined as:

$$\begin{aligned}K(x,x')&=\langle z(x,t)z(x',t)\rangle\\&=\lim_{M\to\infty}\frac{1}{M}\sum_{l=1}^{M}z_l(x)z_l(x')\end{aligned} \tag{47}$$

This function measures the persistent spatial structures that appear in the time series with coherence between x and x'. Using it as a kernel in the following eigenvalue problem for an integral operator:

$$\int K(x, x')\psi_i(x')dx = \mu_i\psi_i(x) \tag{48}$$

we can then reproduce the most dominant coherent structure $\psi_i(x)$ in the system. Since $K(x, x') = K(x', x)$, the integral operator is self-adjoint and hence $\{\psi_i\}$ is an orthonormal basis and $\{\mu_i\}$, the empirical eigenvalues, are positive real eigenvalues. It can be shown (Sirovich, 1987) that μ_i represents the projection of the mean fluctuation energy on the ψ_i basis. Hence, we can now measure the degree of approximation of z by z_N in Eq. 37 by examining how close:

$$E_N = \frac{\sum_{i=1}^{N} \mu_i}{\sum_{i=1}^{\infty} \mu_i} \tag{49}$$

is to unity. For systems with partitioned spectra, such as the one shown in Figure 1, μ_i drops off drastically beyond $i = m$ and the term in the denominator of Eq. 49 can be accurately determined with only a few more terms then m. By the same token, a good estimate of m can be obtained empirically by say:

$$E_m > 0.90 \tag{50}$$

and an estimate of ϵ is then $1 - E_m$. Sirovich (1989) used m in Eq. 50 to estimate the dimension of a chaotic attractor in the same spirit. In essence, the first m modes in Ω_s contain at least 90% of the "energy" and any mode within Ω_f contains less than 1%.

If the linearized operator is like a wave equation:

$$\ddot{z} = L_x z \tag{51}$$

and L_x is self-adjoint with respect to the L_2 inner product, it can be shown by simple integration by parts that the empirical eigenfunction $\{\psi_i\}$ estimated above is identical to the true eigenfunction $\{\phi_i\}$ of L_x. This is not true for systems in the form of Eq. 2. Nevertheless, it demonstrates that $\{\psi_i\}$ roughly resembles $\{\phi_i\}$ and these empirical eigenfunctions are indeed an optimal basis for decomposing the signal. This is verified experimentally in Figures 4 and 5. A total of $M = 183$ snapshots of a two-dimensional infra-red image with 105×68 pixels for the temperature fluctuation on a catalytic wafer for a reaction of CO and Ethylene oxidation recorded from E. E. Wolf's laboratory in our department (Kellow and Wolf, 1991). The temperature fluctuation is due to intrinsic kinetic and thermal instabilities. The first six empirical eigenfunctions from the snap shots are shown in Figure 5 with $(\mu_1, \mu_2, \mu_3, \mu_4, \mu_5, \mu_6) = (61.67, 14.37, 9.72, 3.67, 3.02, 0.95)$ and hence $E_5 = 0.925$, the first five empirical eigenfunctions capture 92.5% of the energy. In Figure 4, we faithfully reconstruct some of the original snapshots with only the first five empirical eigenfunctions using the coefficients c_i indicated in the caption. It is hence evident that instead of requiring 105×68 pixels, the image can be accurately reconstructed with 5 coefficients, a data compression of $O(10^3)$. This is because the temporally chaotic chemical dynamics excites only five coherent structures. Since the dynamics is weakly nonlinear, that is, the fluctuations are localized in a small neighborhood of the equilibrium state this also implies there are only five dominant eigenmodes ($m = 5$) by criterion Eq. 50. Hence, we are able to establish spectrum partition and determine the number of dominant modes m in Ω_s for an actual system.

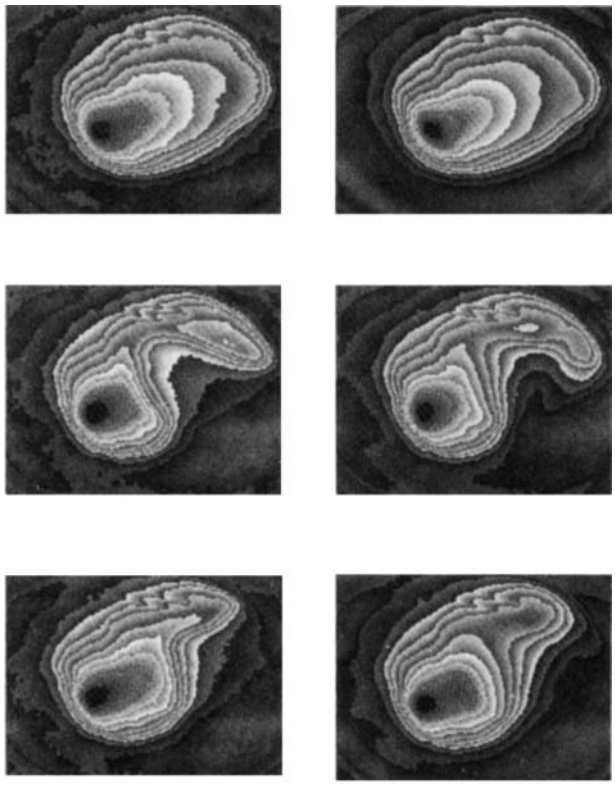

Figure 4. Three typical snapshots from an IR video image of a catalytic wafer on the left and the reconstructed image on the right using the first five empirical eigenfunctions in Figure 5.

The expansion coefficients are $c = (-2.05 \times 10^{-2}, -1.38 \times 10^{-2}, -1.86 \times 10^{-3}, 4.53 \times 10^{-3}, 1.68 \times 10^{-1})$, $(-2.76 \times 10^{-2}, 3.00 \times 10^{-2}, 6.84 \times 10^{-2}, 0.345, -2.99 \times 10^{-2})$ and $(-2.52 \times 10^{-2}, 4.68 \times 10^{-2}, 7.66 \times 10^{-2}, 8.82 \times 10^{-2}, 3.54 \times 10^{-3})$.

Examples

$m = 1$

Our first example is a simple contrived system whose slow spectrum Ω_s contains a lone real eigenvalue

$$\frac{1}{\epsilon}\dot{z} = \pi^2 \frac{\partial^2 z}{\partial x^2} + 9.5z + 0.135\, z^2 + z\frac{\partial z}{\partial x} + xu \tag{52a}$$

$$z(x=0) = z(x=\pi) = 0 \tag{52b}$$

The capacitance factor ϵ^{-1} is a result of rescaling time such that λ_{m+1}^r is $O(1)$ as in Figure 1 to be consistent with our notation. The eigenvalues of the self-adjoint operator $L_x = \epsilon(\pi^2 \partial^2/\partial x^2 + 9.5\, z)$ are:

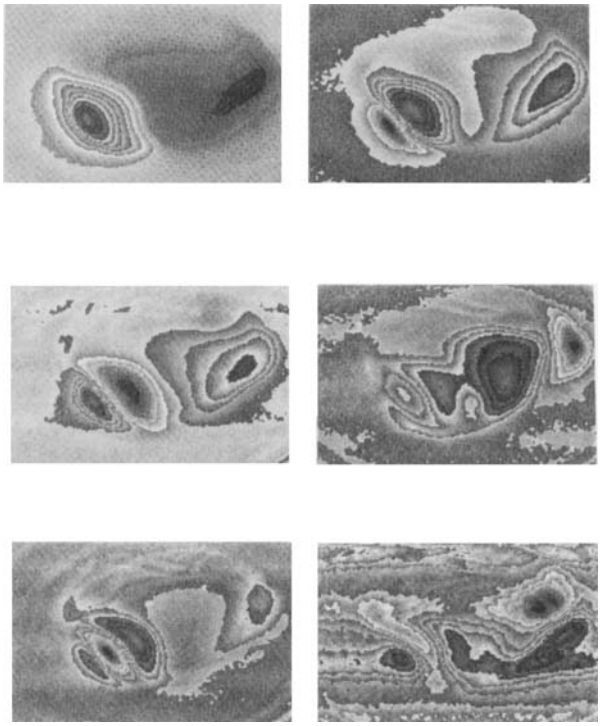

Figure 5. The estimated empirical eigenfunctions from $M = 300$ snapshots.

The empirical eigenvalues are $\mu_i = (61.67, 14.37, 9.72, 3.67, 3.02, 0.95)$ yielding $E_i = (0.617, 0.761, 0.858, 0.894, 0.925, 0.935)$ and an estimate of the dimension of Ω_s $m = 5$.

$$\lambda_i = (9.5 - i^2\pi^2)\epsilon \tag{53a}$$

with eigenfunctions and adjoint eigenfunctions

$$\phi_i = \sin ix \tag{53b}$$

We hence choose ϵ to be 1/50 such that $\lambda_1 = -0.007$ and $\lambda_2 = -0.600$. The equilibrium state here is zero exactly and the feedback law of Eq. 29 becomes

$$u = \epsilon u' = -\epsilon k_L(z, \hat{\phi}_1) - k_N(z, \hat{\phi}_1)^3 \tag{54}$$

where k_L and k_N are of $O(1)$. We numerically integrate Eq. 52 using a pseudo-spectral scheme with the following basis functions:

$$f_i(x) = \sin ix \tag{55}$$

and use the simulated data in our estimation scheme for $\{\psi_i\}$. The response of the system to a random white noise with a characteristic time scale of 0.01 and a maximum amplitude of 10^{-4} is used. The first four empirical eigenfunctions obtained from snapshots at a time interval of $\Delta t = 3$ are shown in Figure 6a and their empirical eigenvalues are $\{\mu_i\} = (9.80 \times 10^{-2}, 6.46 \times 10^{-3}, 2.83 \times 10^{-4}, 6.46 \times 10^{-6}, 4.77 \times 10^{-8}, 1.02 \times 10^{-9})$. Clearly, $m = 1$ according to criterion Eq. 50 and the first mode contains more than 90% of the energy, reflecting the large separation of time scales. We note that the empirical eigenfunctions resemble the true system eigenfunctions of sin ix but

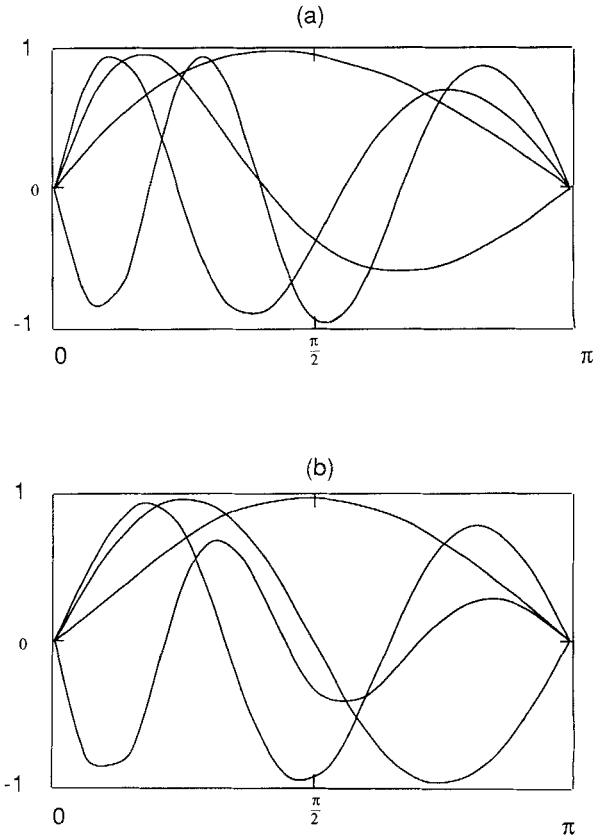

Figure 6. Empirical eigenfunctions $\{\psi_i\}$ and system eigenfunctions $\{\phi_i\}$ estimated from the first example.

a. They resemble skewed versions of the true eigenfunctions $\{\phi_i\}$ with a shift to the left.

b. The shift has been corrected but error persists in the fast modes in Ω_f. This underscores the danger of using feedback containing the fast modes.

are not exactly identical. The difference increases with i. Using these four empirical eigenfunctions to decompose the response of the system to a large step perturbation in u, we are able to estimate A as

$$A = \begin{bmatrix} 0.992 & -3.71 \times 10^{-2} & 7.53 \times 10^{-3} & 5.27 \times 10^{-4} \\ -3.75 \times 10^{-2} & 0.6807 & -0.137 & 1.012 \times 10^{-2} \\ -1.63 \times 10^{-2} & -0.135 & 0.425 & 0.131 \\ 5.22 \times 10^{-3} & 9.7 \times 10^{-3} & 0.131 & 0.262 \end{bmatrix} \tag{56}$$

with estimated eigenvalues $(\lambda_i) = (-0.0075, -0.599, -1.612, -3.467)$ compared to the true eigenvalues $(-0.0074, -0.600, -1.587, -2.968)$. It is obvious that the leading eigenvalues can be estimated very accurately. This confirms that slow modes dominate in the linear region and can be identified correctly. Attempts to identify the fast modes will be in vain and this may even corrupt our identification of the system eigenfunctions and adjoint eigenfunctions because the eigenvectors and adjoint eigenvectors of Eq. 45 will contain components from the inaccurately estimated fast modes. It is advisable, from our experience, to use only the first two empirical eigenfunc-

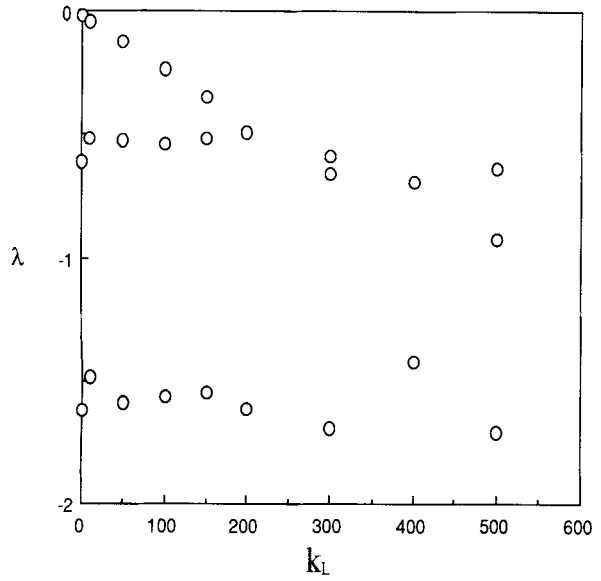

Figure 7. Closed-loop spectrum as a function of linear gain k_L.

Coupling due to measurement error of $\{\phi_i\}$ in Figure 6 is evident for large $k_L \sim O(\epsilon^{-1})$. The relatively small error in estimating ϕ_1 allows an unusually large linear gain.

tions in the identification stage if the codimension k is 1. The linear dynamics is identified when the coefficients $c_i(t)$ in Eq. 37 behave linearly. This is essentially the flat region III portion of Figure 9 near the origin where the projection is on ϕ_i rather than ψ_i. The adjoint eigenfunctions constructed from A in Eq. 56 are shown in Figure 6b. Note that the leading adjoint eigenfunction sin x is estimated virtually exactly while the estimation error increases with i. Note also the maximum of the first empirical eigenfunction in Figure 6a is shifted slightly from the middle but this is corrected in the final estimate in Figure 6b. The resemblance of $\{\psi_i\}$ to $\{\phi_i\}$ is also reflected in the diagonal dominance of A.

We use the estimated $\hat{\phi}_1$ in Figure 6b in the feedback law of Eq. 54. In Figure 7, we depict the closed-loop eigenvalues as a function of k_L. (They are independent of k_N.) As is evident the dominant mode in Ω_s is shifted while Ω_f remains intact for $k_L \sim O(1)$. However, at large gain, $k_L \sim 200 \sim O(\epsilon^{-1})$, coupling occurs as the dominant mode is shifted into Ω_f. Although the coupling for this example seems to shift the Ω_f spectrum further to the left in the complex plane, it can in principle also destabilize Ω_f. Hence, it is important to have only weak linear feedback with $k_L \sim O(1)$. The importance of nonlinear feedback is shown in Figures 8a and 8b by isolating linear and nonlinear feedback. In Figure 8a, only linear feedback is used and as is evident and predicted in Figure 3, linear feedback does not affect the algebraic decay portion and only increases the decay rate of exponential decay in the linear region III. As a result, large-amplitude perturbation is poorly modulated. Beginning at the same initial condition, the closed-loop signal with a large linear gain of $k_L = 50$ is only 28% smaller than the open-loop signal at $t = 225$. With nonlinear feedback shown in Figure 8b, the algebraic decay is accelerated and the closed-loop signal with $k_N = 50$ is 92% lower than the open-loop response at $t = 225$! Note that because there is no linear feedback,

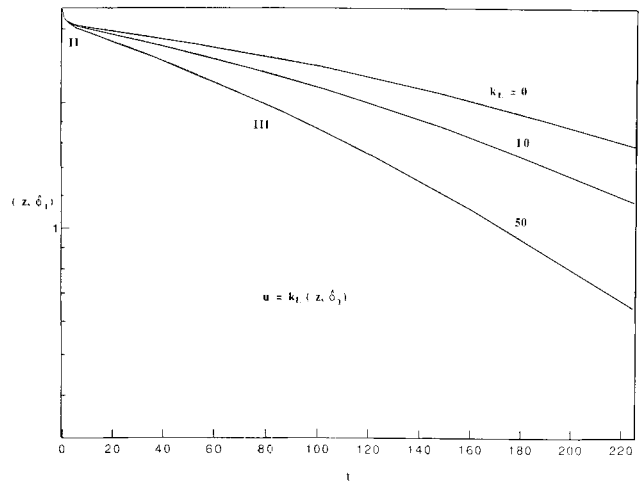

Figure 8a. Accelerated exponential decay in region III due to linear feedback.

The algebraic decay region II is unaffected by linear feedback.

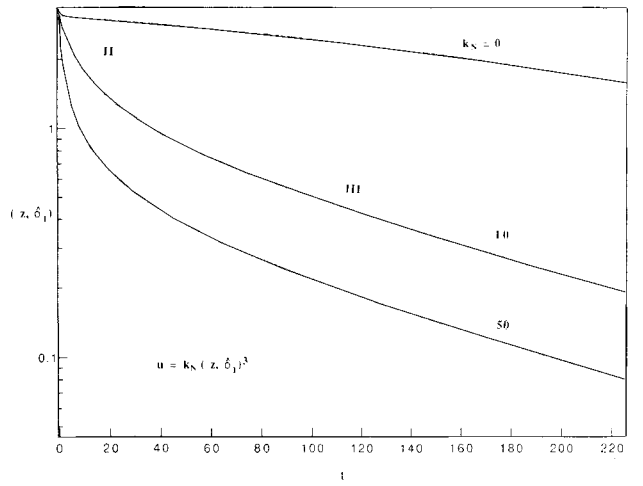

Figure 8b. Nonlinear feedback accelerates the convergence in region II.

Since there is no linear feedback, the decay rate at large time in region III remains independent of k_N.

the linear closed-loop response at large time has the same decay rate for all k_N in Figure 8b. However, the accelerated damping at large amplitude due to nonlinear feedback has already successfully modulated the disturbance at that point. Figures 8a and b hence verify the scenario predicted in Figure 3. In Figure 9, we demonstrate that the invariant manifold M is independent of k_L and k_N if they are both of $O(1)$. It is also noted that if k_N is negative, the origin can loose its asymptotic stability as γ_3 becomes positive. The effect of k_L on the trajectories in Figure 9 is negligible and the k_L values are not shown. The various regions shown in Figure 2 are also marked here.

$m = 2$ - a chemical reactor

For a more complicated and realistic example, we study a packed bed reactor example with $m = n = 2$. Consider the following reactor with a first-order, irreversible, exothermic re-

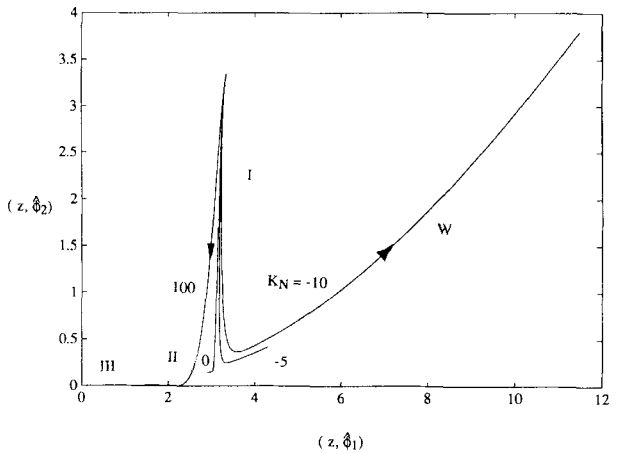

Figure 9. Convergence to the invariant manifold *W* for various values of k_L and k_N.

The phase plane trajectories are insensitive to k_L and only slightly more sensitive to k_N although the velocity on the trajectories is sensitive to k_L and k_N as evident in Figure 8. The origin loses asymptotic stability for a sufficiently negative k_N. Note also the invariance of W with respect to k_L and k_N.

action (Alvarez et al., 1981):

$$\dot{z}_1 = \frac{\partial^2 z_1}{\partial x^2} - Pe_m \frac{\partial z_1}{\partial x} - \alpha z_1 e^{\delta(1-1/z_2)} \tag{57a}$$

$$\dot{z}_2 = \frac{1}{\text{Le}} \frac{\partial^2 z_2}{\partial x^2} - Pe_h \frac{\partial z_2}{\partial x} + \alpha\beta z_1 e^{\delta(1-1/z_2)} + \gamma(T_s - z_2) + T_w u \tag{57b}$$

with boundary conditions:

$$\frac{\partial z_1}{\partial x} = Pe_m(z_1 - z_1^r) \quad \text{at} \quad x = 0 \tag{57c}$$

$$\frac{\partial z_2}{\partial x} = Pe_h(z_2 - z_2^r) \quad \text{at} \quad x = 0 \tag{57d}$$

$$\frac{\partial z_1}{\partial x} = \frac{\partial z_2}{\partial x} = 0 \quad \text{at} \quad x = 1 \tag{57e}$$

where Pe_m and Pe_h are the mass and heat Peclet numbers, z_1 is the concentration, z_2 is the temperature, Le is the Lewis number, α is the Damköhler number, β the heat of reaction, δ the activation energy, γ the heat-transfer coefficient between the reactor and a cooling jacket T_w is the reference spatially uniform coolant temperature within the cooling jacket, z_1^r and z_2^r are at feed conditions and u is selected to be the coolant temperature which is spatially uniform. Our operating condition is selected to be

$$\begin{aligned} &Pe_m = Pe_h = 5 && \delta = 25 \\ &\alpha = 0.875 && T_w = 1 \\ &\beta = 0.5 && z_1^r = 1 \\ &\gamma = 13 && z_2^r = 1.01 \end{aligned} \tag{58}$$

We also simulate the dynamics of example with an orthogonal collocation technique using the following basis (Finlayson, 1980) after the coordinate transformation $x' = -x + 1$

$$f_1(x) = 1$$

$$f_2(x) = 1 - 3x^2$$

$$f_3(x) = 1 - 10x^2 + \frac{35}{3}x^4$$

$$f_4(x) = 1 - 21x^2 + 163x^4 - \frac{231}{5}x^6$$

$$f_5(x) = 1 - 36x^2 + 198x^4 - \frac{1{,}716}{5}x^6 + \frac{1{,}287}{7}x^8$$

$$f_6(x) = 1 - 55x^2 + \frac{1{,}430}{3}x^4 - 1{,}430x^6 + \frac{12{,}155}{7}x^8 - \frac{46{,}189}{63}x^{10}$$

$$f_7(x) = 1 - 78x^2 + 975x^4 - 4{,}420x^6 + \frac{62{,}985}{7}x^8 - 8{,}398x^{10} + \frac{96{,}577}{33}x^{12}$$

$$f_8(x) = 1 - 105x^2 + 1{,}785x^4 - 11{,}305x^6 + 33{,}915x^8 - 52{,}003 \times 10^{10} + \frac{1{,}300{,}075}{33}x^{12} - \frac{1{,}671{,}525}{143}x^{14} \tag{59}$$

and the collocation points

$$\begin{aligned} x_1 &= 0.95012 \quad x_2 = 0.28160 \\ x_3 &= 0.45802 \quad x_4 = 0.61788 \\ x_5 &= 0.75540 \quad x_6 = 0.85563 \\ x_7 &= 0.94458 \quad x_8 = 0.98940 \end{aligned} \tag{60}$$

Since the equilibrium state of this system is not trivial, it also needs to be estimated. We introduce white noise of am-

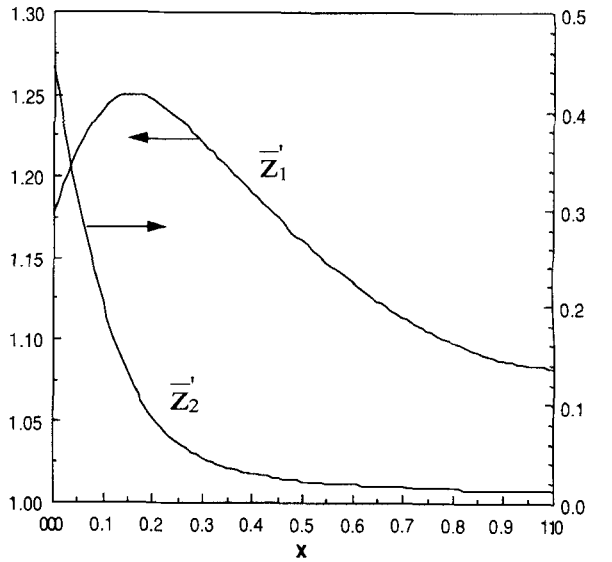

Figure 10. Estimated concentration $\bar{z}_1'$ and temperature $\bar{z}_2'$ profiles of the equilibrium state of the reactor.

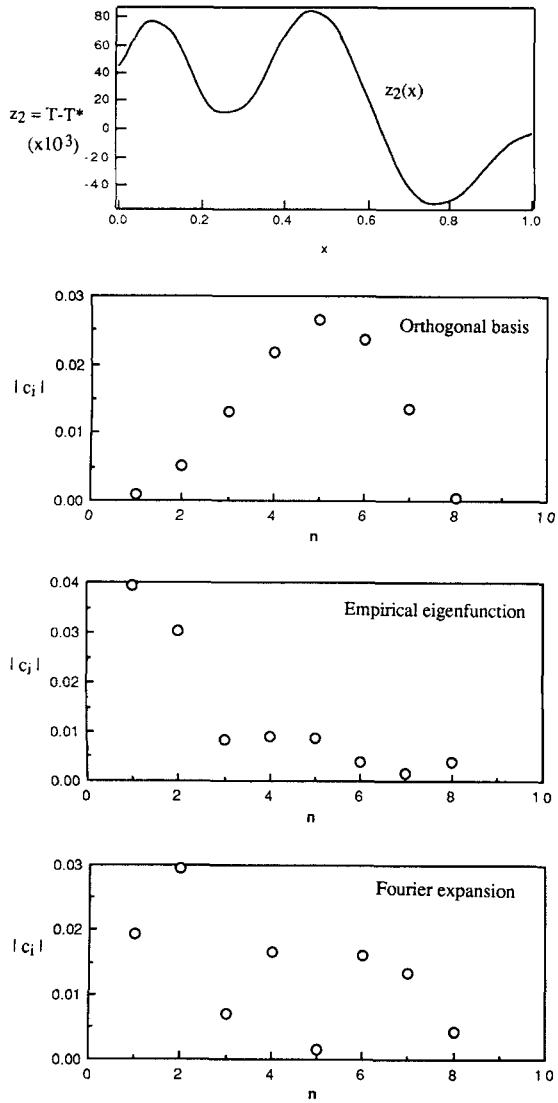

Figure 11. Decomposition of a typical reduced snapshot using three different basis.

The empirical eigenfunction clearly outperforms the more conventional bases.

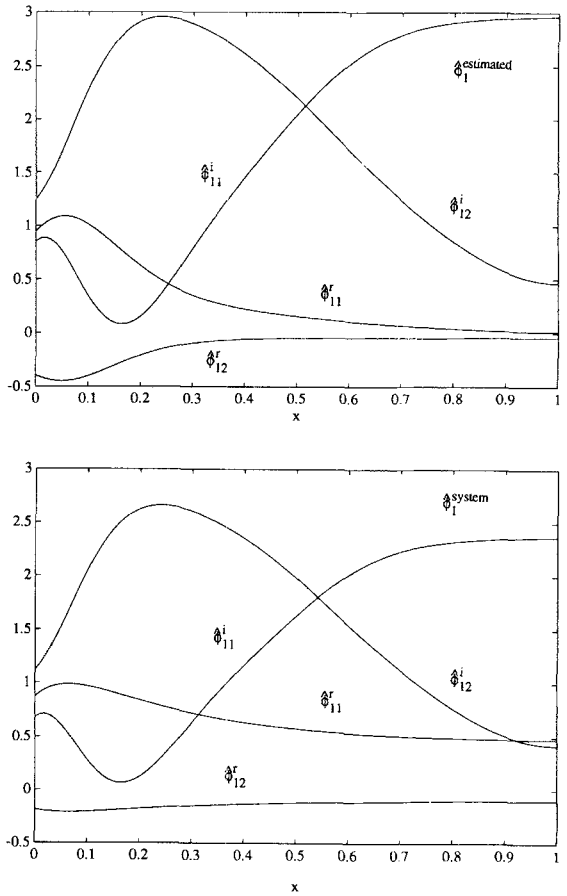

Figure 12. The four elements of the estimated complex adjoint eigenfunction $\hat{\phi}_1 = (\hat{\phi}_{11}, \hat{\phi}_{12}) = (\hat{\phi}^r_{11} + i\hat{\phi}^i_{11}, \hat{\phi}^r_{12} + i\hat{\phi}^i_{12})$.

a. The element $\hat{\phi}_{11}$ corresponds to concentration and $\hat{\phi}_{12}$ to temperature. The location of the hot spot in $\bar{z}^r_2$ of Figure 10 is still evident here in $\hat{\phi}^i_{12}$.

b. The true system adjoint eigenfunction. Some minute quantitative difference can be observed by comparing to (a) but the error is small.

plitude $(\Delta z_1, \Delta z_2) = (10^{-10}, 10^{-10})$ into the system and $M = 300$ snapshots are taken at an interval of $\Delta t = 0.01$. The ensemble average of the snapshots, yields the estimated equilibrium state of Figure 10 which is virtually identical to the actual equilibrium state. The same ensemble of snapshots are used to estimate the empirical eigenfunctions and eigenvalues. The first six empirical eigenvalues are $\{\mu_i\} = \{1.78 \times 10^{-2}, 1.88 \times 10^{-3}, 3.12 \times 10^{-4}, 6.83 \times 10^{-5}, 8.38 \times 10^{-6}, 3.35 \times 10^{-6}\}$ and it is clear from criterion Eq. 50 that $m = 2$. To show that these empirical eigenfunctions are the optimal basis for the system, we decompose a typical reduced snapshot in Figure 11 with an orthogonal basis of Eq. 59, the empirical eigenfunctions and a finite Fourier expansion. It is clear that the convergence is most rapid with the empirical eigenfunction with only two modes necessary. Using the first two empirical eigenfunctions, we estimated A from large-time open-loop step responses, making sure that the trajectory has settled onto a plane containing the origin in the c_i space,

$$A = \begin{pmatrix} 0.9537 & 0.2454 \\ -0.0380 & 0.9539 \end{pmatrix} \tag{61}$$

This yields the estimated open-loop leading eigenvalues $\lambda_{1,2} = -2.19 \pm 22.4i$ which are very close to the true eigenvalues $-2.34 \pm 22.46i$. The estimated adjoint eigenfunctions are favorably compared to the true ones in Figure 12. Note that since $n = 2$ and $\hat{\phi}_1$ is complex, there are a total of four real scalar functions in $\hat{\phi}_1(x) = (\hat{\phi}_{11}, \hat{\phi}_{12})$.

The closed-loop spectrum using feedback law Eq. 29 is shown in Figure 13. Again, large linear gain with $k_L \sim O(\epsilon^{-1}) \sim 20$ leads to linear closed-loop coupling between the slow and fast modes such that the leading complex mode breaks up into two real modes. One real mode actually destabilizes for $k_L > 20$. This confirms the wisdom of using weak linear feedback with $k_L \sim O(1)$. The dramatic effect of nonlinear feedback in damping large-amplitude noise in region II is shown in Figure 14. Modulation by several orders of magnitude is evident. The fast fluctuation seen in Figure 14 is due to imperfect projection

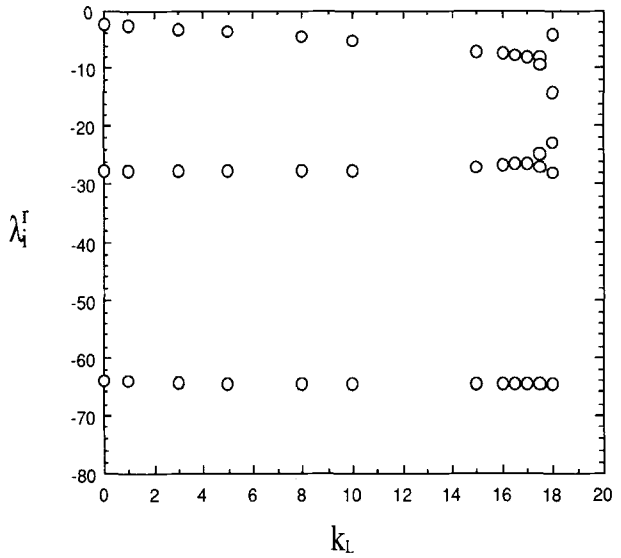

Figure 13. Closed-loop spectrum as a function of linear gain k_L.

Coupling at large k_L gives rise to closed-loop instability here. Because the estimation error shown in Figure 12 is larger than that of the first example in Figure 6, a smaller k_L gives rise to coupling here even though ϵ is about the same for both examples.

in $|(z, \hat{\phi}_1)|$ to remove the phase (oscillatory) portion of the signal represented by Eq. 26b. The oscillations have characteristic frequency of ~ 0.3 Hz corresponding to λ_1^i. The actual damping of a large-amplitude spatially distributed disturbance is shown in Figure 15. A hot spot excursion is shown to be arrested by our nonlinear feedback. Since we only used 8 orthogonal polynomial basis in our simulation, the fluctuations do not have fine spatial structure. However, this is only a weakness of the numerical experiment. Our scheme is fully capable of filtering out short scale noise and retaining fine structures in the dominant eigenfunctions as evident in Figures 4 and 5.

Summary and Discussion

We have developed a new approach to controlling nonlinear distributed systems with unknown dynamics. It pertains to systems with a partitioned spectrum but we argue that such systems are ubiquitous in chemical processes with different time scales. An identification scheme is developed to identify such systems and to estimate the dominant adjoint eigenfunctions in Ω_s. It exploits the optimal basis of empirical eigenfunction. It is then shown, both analytically and numerically, that a finite-amplitude disturbance can be damped with a smooth nonlinear feedback law which requires only information on the dominant adjoint eigenfunctions. The actual nonlinear physical model is unnecessary. Asymptotic stability is ensured by our scheme provided that linear feedback is weak. The nonlinear gain can be large, however, and we demonstrate dramatic performance improvement over linear feedback.

Although we did not explicitly discuss a possible tuning strategy for controller gains k_L and k_N, the existence of optimal gains is already implicit in our discussion. The performance of our scheme obviously increases with both gains if the system dynamics is accurately identified from our time series. How-

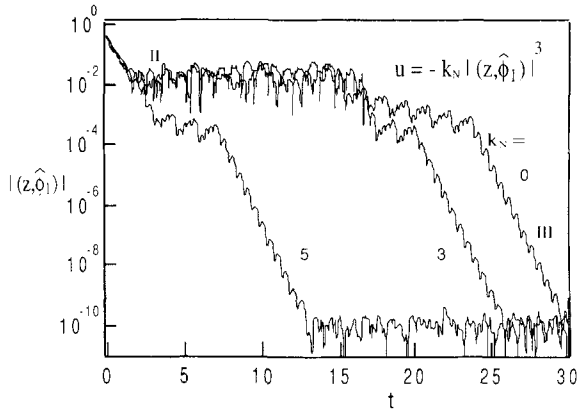

Figure 14. Accelerated convergence due to nonlinear feedback only which does not alter the decay rate in region III.

ever, as shown in our two examples, there is a coupling between the fast and slow modes at a large gain of $O(\epsilon^{-1})$ such that the number of dominant modes m increases. If the identification scheme is not altered adaptively to account for this large-gain effect, destabilization can occur. This then implies that, for a given identification scheme, an optimal gain setting exists. On the other hand, our identification scheme can easily adapt to changes in m due to this feedback-induced coupling or due to process dynamic changes. Consequently, the optimal gains can be arbitrarily large which is, of course, a major advantage of this approach. Robustness of our identification scheme allows us to determine the eigenfunctions on-line adaptively in parallel with the feedback loop. A constant updating of the most dominant eigenfunctions is hence possible to allow continuous large-gain feedback. Tuning is then unnecessary or even inappropriate.

If an obvious partition of the spectrum does not exist, our approach will alter the dynamics on an invariant manifold which is a nonlinear extension of the eigen vectors of Ω_s. Some derivation, such as the smallness of the real part of Λ_s stipulated in Eq. 13 will be different but the final equations describing

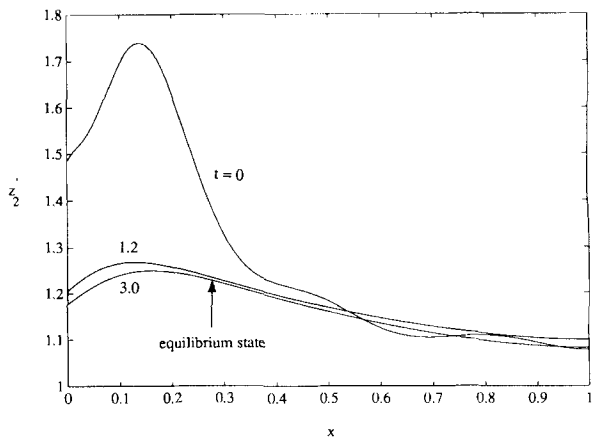

Figure 15. Arresting a large-amplitude hot-spot excursion with our nonlinear feedback with (k_L, k_N) = (0.1, 3).

The unreduced temperature profile is shown at various time.

the closed-loop dynamics on the invariant manifold still resembles Eq. 31. The problem, however, is that the system does not approach the invariant manifold rapidly and the uncontrolled linear and nonlinear dynamics of Ω_f is just as important as the faster modes in Ω_s. It then becomes a matter of including sufficient modes in Ω_s such that the dynamics of Ω_f becomes insignificant. In this connection, we note that we have only developed the theory for the codimension one case with a lone dominant eigenvalue or a dominant pair. However, extension to higher codimensions is quite straightforward provided multiple inputs are allowed to ensure asymptotic stability with proper signs for all the Landau coefficients in the slow equation and independent movements of the dominant eigenvalues.

The problem arises, however, in the estimation scheme for too large an Ω_s spectrum. The estimates of the dominant eigenfunctions ψ_i deteriorate with i and a large m or k will introduce more errors. It should be reminded that any finite-dimensional approximation of a distributed system implicitly uses a separation of scales argument that omits all higher modes. Unfortunately, most of these approximations involve too large a slow spectrum Ω_s to allow reconstruction from our estimation scheme. A possible strategy is to shift the leading eigenvalues in Ω_s to its left boundary sequentially. Only the dominant ones in Ω_s will be shifted first since they are most accurately identified. Once shifted, a second set becomes dominant. They are identified next and shifted by an additional feedback. In this manner, a large Ω_s spectrum may still be identified accurately. We have also assumed that the distributed signal $z(x,t)$ is accurately resolved in both space and time. This, of course, assumes sufficient number of sensors and sufficiently rapid sensor response. In this respect, we believe that video imaging using IR cameras such as those used in Figures 4 and 5 offer almost perfect resolution due to the large number of pixels.

With the availability of fast digital video cameras and image processors, it is not overly optimistic to envision the use of video images as temperature sensors in real-time feedback control. Nor is our assumption of weak nonlinearity a difficult obstacle to possible extension to strongly nonlinear dynamics. The original empirical eigenfunction approach of deciphering coherent structures is not restricted to small fluctuations. However, with strongly nonlinear dynamics, the coherent structures no longer resemble the eigenmodes and the weakly nonlinear analysis of the second section is not valid. A different approach must then be developed to decipher the slow dynamics of the coherent structures. Since the convenient form of the slow equation in Eq. 31, is now unavailable, we suspect some estimation of the nonlinear dynamics of the coherent structures becomes necessary. This will complicate the approach. Another factor that may require nonlinear modeling is our current assumption that all state variables are measurable. If only a subset of them can be measured, the others most likely must be estimated. This is probably the most important issue that should be resolved next. In such schemes for estimating the nonlinear dynamics, modern time series tools such as time-delayed embedding and neural net/parallel processing techniques should prove important (Hudson et al., 1990; Boe and Chang, 1991).

Acknowledgments

We are grateful to Professor E. E. Wolf for allowing us to analyze his data in Figures 4 and 5. This work was supported by the National Science Foundation under grants NSF CBT 8451116 and NSF CTS-9112977.

Notation

A = discrete version of $\tilde{A}$
$\tilde{A}$ = Jacobian of linearized system
a_i = amplitudes of eigenmodes
B, C, D, E, F = coefficients of $f(a_s, a_f)$ and $g(a_s, a_f)$
b = premultiplied constant of u
c = projection of z onto ψ
c_i = components of c
D, T = bilinear and trilinear operators
Em = energy percent occupied by first m mode
E' = constant tensor
$f(a_s, a_f), g(a_s, a_f)$ = nonlinear functions of a_s and a_f
f_i = basis functions
g_i = constants
h = nonlinear transformation
J = cost function
k = codimension
K = two-point spatial correlation function
k_L, k_L', k_N = linear, unscaled linear and nonlinear gains
Le = Lewis number
L_x, L_x^+ = differential and adjoint operator
M = center manifold
$N(z)$ = nonlinear spatial vector function
P, Q = matrices used to find A
Pe_h, Pe_m = mass and heat Peclet number
r_i = amplitudes of invariant or center manifold
Tw = coolant temperature
Δt = sampling time
u = feedback control
u_i = components of u
v = coordinate transformation of w
V = Lyapunov function
w = dynamics of center manifold
W = invariant manifold
x = spatial coordinate
x' = transformed spatial coordinate, $x' = -x+1$
x_i = collocation points
z = distributed variable
z_1, z_2 = concentration and temperature
z_1', z_2' = inlet concentration and temperature
z_i = components of z
z_l' = on-line measurement of z at $t = l(\Delta t)$
$\bar{z}'$ = time-averaging of z'
z_l = reduced variable, $z_l = z_l' - z'$
$\Delta z_1, \Delta z_2$ = maximum noise amplitudes

Greek letters

α = Damköhler number
α_i = coefficients of center manifold Eq. 22
β = spatial matrix function or heat of reaction
δ = small parameter of identification error or activation energy
δ_2, δ_3 = closed-loop version of γ_2 and γ_3
ϵ = small parameter, $\epsilon = |\lambda_1'/\lambda_{m+1}'|$
ϕ_i = system eigenfunctions
$\hat{\phi}_{11}, \hat{\phi}_{12}$ = complex leading eigenfunctions of concentration and temperature
γ_2, γ_3 = Landau coefficients
Λ = diagonal eigenvalue matrix
Λ_r, Λ_i = real and imaginary part of Λ
λ = system eigenvalue
$\tilde{\lambda}$ = eigenvalue of $\tilde{A}$
μ_i = empirical eigenvalues
θ = phase of v
Ω = eigen spectrum
ω = imaginary part of λ_1
ψ_i = empirical eigenfunctions

Superscripts

r = real part
i = imaginary part
$-$ = complex conjugate

Subscripts

s = slow mode
f = fast mode

Literature Cited

Aluko, M., and H.-C. Chang, "Multi-Scale Analysis of Exotic Dynamics in Surface Catalyzed Reactions I and II," *Chem. Eng. Sci.*, **39**, 37, **39**, 51 (1984).

Alvarez, J. J., A. Romagnoli, and G. Stephanopoulos, "Variable Measurement Structures for the Control of a Tubular Reactor," *Chem. Eng. Sci.*, **36**, 1695 (1981).

Boe, E. and H.-C. Chang, "Transition to Chaos from a Two-Torus in a Delayed Feedback System," *Int. J. of Bifurcation and Chaos*, **1**, 67 (1991).

Carr, J., *Application of Centre Manifold Theory*, Springer-Verlag (1981).

Crawford, J., "Hopf Bifurcation and the Beam-Plasma Instability," *Contemporary Mathematics*, **28**, 377 (1984).

Finlayson, B. A., *Nonlinear Analysis In Chemical Engineering*, McGraw-Hill (1980).

Foias, C., M. S. Jolly, I. G. Kevrekidis, G. R., Sell, and E. S. Titi, "On the Computation of Inertial Manifolds," *Phys. Lett.*, **A131**(8), 433 (1988).

Gay, D. H, and W. H. Ray, "Identification and Control of Linear Distributed Parameter Systems through the use of Experimentally Determined Singular Functions," *Proc. of IFAC Symposium on Control of Distributed Parameter Systems* (1986).

Gay, D. H., and W. H. Ray, "Application of Singular Value Methods for Identification and Model/Based Control of Distributed Parameter Systems," *Proc. of IFAC Workshop in Model Based Process Control* (1988).

Guckenheimer, J., and D. Holmes, "Nonlinear Oscillations, Dynamical Systems, and Bifurcations of Vector Fields," Springer-Verlag (1983).

Hudson, J. L., M. Kube, R. A. Adomaitis, I. G. Kevrekidis, A. S. Lapedes, and R. M. Farber, "Nonlinear Signal Processing and System Identification: Applications to Time Series from Electrochemical Reactions," *Chem. Eng. Sci.*, **45**(8), 2075 (1990).

Hwang, S. H., and H.-C. Chang, "Turbulent and Inertial Roll Waves in Inclined Film Flow," *Phys. Fluids*, **30**, 1259 (1987).

Iooss, G., and D. D. Joseph, *Elementary Stability and Bifurcation Theory*, Springer-Verlag (1980).

Kellow, J. C, and E. E. Wolf, "Propagation of Oscillations During Ethylene Oxidation on Rh/SiO_2 Catalysts," *AIChE J.*, **37**(12), 1844 (1991).

Kravaris, C., and J. C. Kantor, "Geometric Methods for Process Control. 1. Background and 2. Synthesis," *IEC Research*, **29**, 2295, 2310 (1990).

Khorasani, K., and P. V. Kokotovic, "A Corrective Feedback Design for Nonlinear Systems with Fast Actuators," *IEEE Trans. on Auto. Control*, **AC-31**, 67 (1986).

Kokotovic, P. V., and P. W. Sauer, "Integral Manifold as a Tool for Reduced-Order Modeling of Nonlinear System: A Synchronous Machine Case Study," *IEEE Trans. on Circuits and Systems*, **36**(3), 403 (1989).

Loeve, M., *Probability Theory*, Van Nostrand (1955).

Lumley, J. L., *Stochastic Tools in Turbulence*, Academic Press, New York (1970).

McDermott, P. E,. and H.-C. Chang, "On the Global Behavior of an Auto-Thermal Reactor Stabilized by Linear Feedback Control," *Chem. Eng. Sci,*. **39**, 1347 (1984).

McDermott, P. E., H.-C. Chang, and R. G. Rinker, "Experimental Investigation of Controller-Induced Bifurcations in a Tubular Reaction," *Chem. Eng. Sci.*, **40**, 1355 (1985).

Morari, M, and E. Zafiriou, *Robust Process Control*, Prentice-Hall (1989).

Sirovich, L., "Turbulence and the Dynamics of Coherent Structures, Part I," *Quart. of Applied Math.*, **45**(3), 561 (1987).

Sirovich, L., "Chaotic Dynamics of Coherent Structures," *Physica D*, **37**, 126 (1989).

Sirovich, L., M. Kirby, and M. Winter, "An Eigenfunction Approach to Large-Scale Transitional Structures in Jet Flow," *Phys. Fluids*, **A2**, 127 (1990).

Temam, R., "Inertial Manifolds and Multi-Grid Methods," *SIAM J. Math. Anal.*, **21**(1), 154 (1990).

Titi, E. S., "On Approximate Inertial Manifolds to the Navier Stokes Equation," *J. Math. Anal. Appl.*, **149**(2), 540 (1990).

Manuscript received Jan. 8, 1992, and revision received May 6, 1992.